1 **Effect of NO$_x$ on 1,3,5-trimethylbenzene (TMB) oxidation product distribution and particle**
2 **formation**
3

4 Epameinondas Tsiligiannis[1], Julia Hammes[1], Christian Mark Salvador[1], Thomas F. Mentel[1,2], Mattias
5 Hallquist[1]*
6 [1]Department of Chemistry and Molecular Biology, University of Gothenburg, Gothenburg, Sweden
7 [2]Institute of Energy and Climate Research, IEK-8: Troposphere, Forschungszentrum Jülich GmbH,
8 Jülich, Germany
9 * *Correspondence to*: hallq@chem.gu.se

10 **Abstract**

11 Secondary organic aerosol (SOA) represents a significant fraction of the tropospheric aerosol
12 and its precursors are volatile organic compounds (VOC). Anthropogenic VOCs (AVOC) dominate the
13 VOC budget in many urban areas with 1,3,5-trimethylbenzene (TMB) being among the most reactive
14 aromatic AVOCs. TMB formed highly oxygenated organic molecules (HOM) in NO$_x$ free environment,
15 which could contribute to new particle formation (NPF) depending on oxidation conditions were
16 elevated OH oxidation enhanced particle formation. The experiments were performed in an oxidation
17 flow reactor, the Go:PAM unit, under controlled OH oxidation conditions. By addition of NO$_x$ to the
18 system we investigated the effect of NO$_x$ on particle formation and on the product distribution. We show
19 that the formation of HOM and especially HOM accretion products, strongly varies with NO$_x$ conditions.
20 We observe a suppression of HOM and particle formation with increasing NO$_x$/ΔTMB and an increase
21 in the formation of organonitrates (ON) mostly at the expense of HOM accretion products. We propose
22 reaction mechanisms/pathways that explain the formation and observed product distributions with
23 respect to oxidation conditions. We hypothesize that, based on our findings from TMB oxidation studies,
24 aromatic AVOCs may not contribute significantly to NPF under typical NO$_x$ /AVOC conditions found
25 in urban atmospheres.

26 **1 Introduction**

27 Volatile organic compounds (VOC) are ubiquitous in the atmosphere and major precursors for
28 secondary organic aerosol (SOA). SOA represents a dominant fraction of the tropospheric aerosol
29 (Hallquist et al., 2009;Shrivastava et al., 2017;Gentner et al., 2017) and affects climate
30 (Intergovernmental Panel on Climate, 2014) and health (WHO, 2016). Consequently research interest
31 in SOA formation and properties is ranging from remote atmospheres (Ehn et al., 2012;Ehn et al.,
32 2014;Kristensen et al., 2016) to densely populated and polluted environments (Chan and Yao, 2008;Hu
33 et al., 2015;Guo et al., 2014;Hallquist et al., 2016). Following the study by Ehn et al. (Ehn et al., 2012),
34 highly oxygenated organic molecules (HOM) with low volatilities, formed from the oxidation of
35 biogenic volatile organic compounds (BVOCs), have attracted much research interest (Crounse et al.,
36 2013;Ehn et al., 2014;Jokinen et al., 2014;Jokinen et al., 2015;Mentel et al., 2015;Yan et al.,
37 2016;Berndt et al., 2016;Bianchi et al., 2019). These compounds have been shown to contribute to new
38 particle formation (NPF) and to SOA growth (Ehn et al., 2014;Bianchi et al., 2016;Kirkby et al.,
39 2016;Trostl et al., 2016;McFiggans et al., 2019), making them an important factor in the formation of
40 atmospheric SOA. These oxidation products can be either described as HOM based on their high oxygen
41 number (O> 6) (Bianchi et al., 2019) or as extremely low volatile organic compounds (ELVOC) based
42 on their volatility (Donahue et al., 2012;Trostl et al., 2016). In this study, we will refer to oxidation
43 products as HOM, because not all of the measured compounds may fulfill the criteria for ELVOC (Trostl

44   et al., 2016;Kurtén et al., 2016). Gas phase autoxidation of alkylperoxy radicals (RO_2) has been proposed
45   as the formation mechanism for HOM (Crounse et al., 2013;Ehn et al., 2014;Jokinen et al., 2014). After
46   the initial reaction of an oxidant with the VOC and subsequent addition of O_2 to the alkylradical (R), the
47   produced RO_2 isomerizes via intra molecular H abstraction (H-shift). During this process a
48   hydroperoxide group and a new R is formed. Additional O_2 addition and H-shift sequences can introduce
49   large amounts of oxygen to the molecule and subsequently lower the vapour pressure. The chemistry of
50   aromatic compounds is somewhat different compared to other VOCs as they can lose their aromaticity
51   during the initial OH attack while they can retain the ring structure. Moreover, reaction products are
52   more reactive than the parent compound. The produced RO_2 form an oxygen bridge, a bicyclic and
53   potentially a tricyclic alkylradical (Molteni et al., 2018;Wang et al., 2017) before further oxidation
54   processes open the ring structure. For 1,3,5-trimethylbenzene (TMB), emitted from combustion sources
55   in the urban environment, Molteni et al. (2018) proposed a generalized reaction scheme for HOM
56   formation after OH addition. According to their scheme, first generation alkylperoxy radicals with the
57   general formula of $C_9H_{13}O_{5-11}$ were formed from the initial OH attack and subsequent H shift and O_2
58   addition sequences. A postulated second OH attack would result in propagating peroxy radical chains
59   yielding radicals with the general formulas $C_9H_{15}O_{7-11}$.

60   Generally, the termination reaction of RO_2 (with a general m/z = x) with HO_2, leads to the
61   formation of hydro peroxides (m/z = x +1) while termination reactions with other RO_2 can lead to the
62   formation of a carbonyl (m/z = x -17), a hydroxy group (m/z = x -15) or dimers (m/z = 2x – 32) (Mentel
63   et al., 2015;Jokinen et al., 2014;Rissanen et al., 2014). The propagation reaction of RO_2 with another
64   RO_2 or NO also results in the formation of RO (m/z = x-16). The RO can undergo internal H shift leading
65   to the formation of a hydroxy group and subsequent a new peroxy radical which can continue the
66   autoxidation sequences. The alkoxy step shifts of the observed m/z by 16 leads to overlap of different
67   termination product sequences. During extensive oxidation the first generation products are subject to
68   secondary chemistry increasing the numbers of products. Molteni et al. (Molteni et al., 2018) found
69   several closed shell monomer products with the general formula $C_9H_{12-16}O_{5-11}$ from the oxidation of
70   TMB with OH. The formation of dimers with different number of H atoms in their study was explained
71   by reactions of two first generation RO_2 radicals ($C_{18}H_{26}O_{5-10}$), one first and one second generation RO_2
72   ($C_{18}H_{28}O_{9-12}$) or two second generation RO_2 resulting in the dimer $C_{18}H_{30}O_{11}$. Although dimers have in
73   general lower O:C ratios than monomers, they are expected to be less volatile due to higher molecular
74   weight and more functional groups making them candidates to participate in nucleation processes
75   (Kirkby et al., 2016).

76   Organonitrates (ON) are formed as soon as sufficient NO_x is present in the atmosphere. ON are
77   highly important for the reactive nitrogen budget wherein the formation of highly functionalized organic
78   nitrates can contribute significantly to secondary organic aerosol (Lee et al., 2016;Bianchi et al., 2017).
79   In this study we refer to compounds that only consist of H, C and O as HOM monomers or HOM dimers
80   and to N containing compounds as ONs.

81   NO_x influences the oxidation of organics directly by changing oxidant levels (reducing or
82   increasing OH, depending on the NO_x regime) and indirectly by influencing RO_2 chemistry. In high NO_x
83   environment such as urban areas the reaction of NO with RO_2 radicals can compete with the autoxidation
84   mechanism (reaction 1 and 2) and thus potentially inhibit HOM while favouring some ON formation
85   (reaction 1 with a yield of up to 0.3).

86 $$RO_2 + NO \rightarrow RONO_2 \tag{1}$$

87 $$\rightarrow RO + NO_2 \tag{2}$$
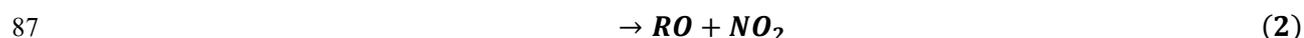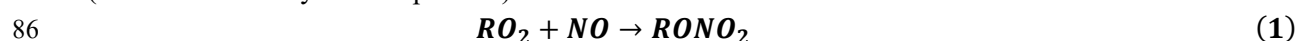
88 Although ON may have high O:C they differ from HOM as they contain at least one nitrogen atom.
89 While HOM formation from BVOCs has been intensively studied, only few studies have been conducted
90 focusing on the formation of HOM from anthropogenic aromatic volatile organic compounds (AVOCs)

(Molteni et al., 2018;Wang et al., 2017). However, these studies indicate that AVOCs have a strong potential to form HOM under NO_x free conditions and proposed that they may play a crucial role in NPF and particle growth of SOA in urban areas. Regarding SOA yields a number of smog chamber studies have been conducted in order to investigate the oxidation of TMB with OH radical under different NO_x and aerosol seed conditions (Paulsen et al., 2005;Rodigast et al., 2017;Wyche et al., 2009;Huang et al., 2015;Sato et al., 2012). They reported that under higher NO_x:VOC conditions, SOA yield is reduced compared to medium or lower NO_x:VOC conditions. The NO_x:VOC, in almost all studies, was < 1, apart from one experiment (Wyche et al., 2009), with NO_x:VOC = 1.9 in which the SOA yield was 0.29, compared to yields up to 7.47 under lower NOx conditions.

In this study we investigate the oxidation of TMB in a laminar flow reactor, while different NO_x and OH conditions were applied. A nitrate chemical ionization atmospheric pressure interface time of flight mass spectrometer (CI-APi-TOF-MS) (Junninen et al., 2010;Jokinen et al., 2012) was used to monitor the oxidation product distribution. We show the formation of HOM and nitrate containing compounds with and without NO_x added to the reaction system. . Possible mechanisms leading to the formation of ON and suppression of particle formation are discussed.

2   Materials and Methods

The measured HOM were generated using the laminar flow Gothenburg Potential Aerosol Mass reactor (Go:PAM), initially described by Watne et al. (Watne et al., 2018). The Go:PAM is a 100 cm long, 9.6 cm wide quartz glass cylinder which is irradiated over a length of 84 cm by two 30 W Phillips TUV lamps (254 nm); a schematic is shown in Figure 1. The OH radicals are produced inside Go:PAM by photolysing O_3 in the presence of water vapour. The O_3 is generated outside Go:PAM by photolyzing pure O_2 (UVP Pen-Ray® Mercury Lamps, 185 nm) and distributed in 3 L min^{-1} particle free and humidified air (Milli – Q) over the reactor cross section. The VOC was introduced through a gravimetrically characterized diffusion source (see Figure S2) centrally at the top of the reactor with a flow of 8 L min^{-1} while NO was introduced via a NO gas cylinder. Flows were adjusted for a median residence time of 34 s in Go:PAM. A funnel shaped device is subsampling the centre part of the laminar flow to minimize wall effects on the sample. A condensation particle counter (CPC, 3775 TSI) was used to measure the number particle concentration in the sample flow. O_3 was monitored by a model 202 monitor (2B Technologies), relative humidity by a Vaisala HMP60 probe and NO_x by a model 42i monitor (Thermo Scientific) over the course of the experiments. The OH exposure, over the residence time in the reactor, for NO_x free conditions without added TMB was measured using SO_2 titration (Teledyne T100) as described by Kang et al. (Kang et al., 2007). Gas phase oxidation products were measured with an Atmospheric Pressure interface High Resolution Time of Flight Mass Spectrometer (APi-TOF-MS, Aerodyne Research Inc. & Tofwerk AG) (Junninen et al., 2010;Jokinen et al., 2012) in connection with a A70 CI-inlet (Airmodus Ltd) (Eisele and Tanner, 1993). The CI inlet is a laminar flow inlet operated with a sheath flow of 20 L min^{-1} containing NO_3^- ions which are generated by ionizing HNO_3 using an [241]Am foil upstream in the inlet design. The sample stream from Go:PAM is introduced in the centre of the sheath flow at a rate of 8 L min^{-1}. The NO_3^- ions are electrostatically pushed into the sample flow and form stable adducts with sample molecules as described by Ehn et al. (2012). The reaction time of oxidation products and NO_3^- is a few hundred ms before being subsampled into the TOF-MS at 0.8 L min^{-1} by a critical orifice. Differential pumping decreased the pressure from 103 mbar in the CI source to 10^{-6} mbar in the TOF extraction region where HOM are detected as negatively charged clusters with NO_3^-.
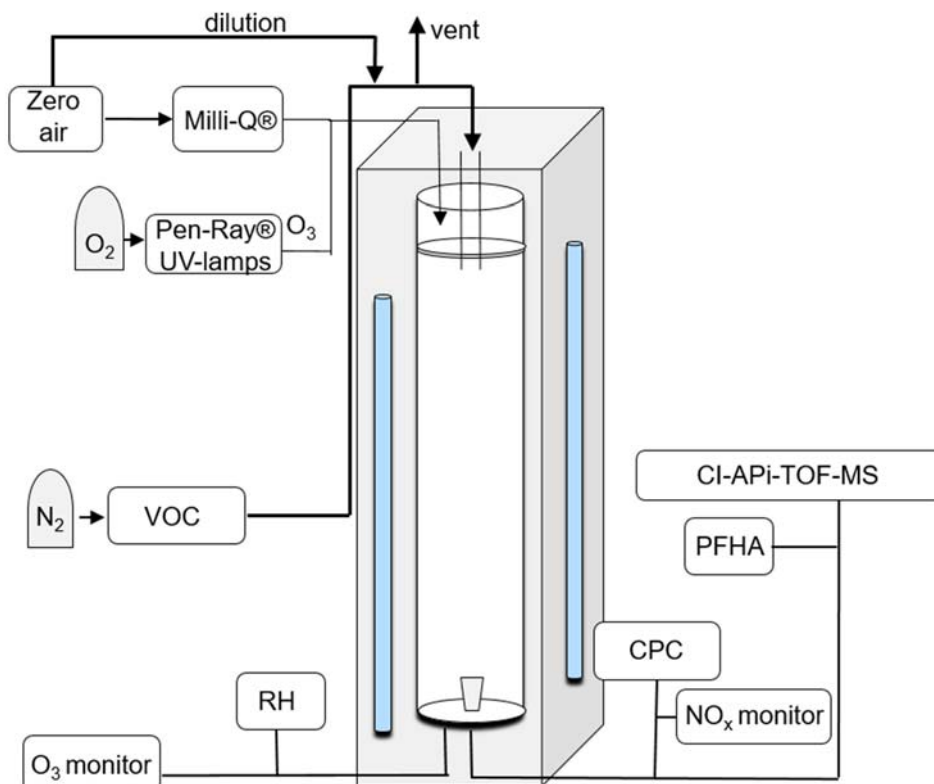
134
135 **Figure 1: Schematics of the experimental setup with Go:PAM chamber connected to CI- APi-**
136 **TOF-MS.**

137   A kinetic box model was used to simulate the chemistry in the Go:PAM reactor. The core of the
138 model were first described by Watne et al. (Watne et al., 2018). The model consists of 32 species and
139 68 reactions now including TMB chemistry partly from the MCM v3.3.1 (Jenkin et al., 2003) as well as
140 proposed mechanisms and rate coefficients for NO_2 chemistry (Atkinson et al., 1992;Finlayson-Pitts,
141 1999) and highly oxygenated compounds (Ehn et al., 2014; Berndt et al., 2018; Zhao et al., 2018) (see
142 SI Table S2). The photon flux used in the simulations was tuned to match measured decay of O_3 while
143 an OH sink was added to match the observed OH exposure in the background experiment, i.e. without
144 the addition of TMB. The model was run for all experiments with and without NO_x. Primarily, the
145 modelled output on OH exposure for each experiments was used to interpret the results and for
146 calculating the consumed TMB. However, broadly the modelling output was also used to understand
147 the effects of changing experimental conditions on monomer, dimer and organonitrate (ON) production.
148 The experiments without NO_x were named 1-4 denoting the increase in OH exposure and experiments
149 with NO_x were denoted according to their NO_x/ ΔTMB and high (H) and low (L) OH exposure as seen
150 in Table 1.

151 **3   Results and Discussions**

152   Table 1 summarises eight experiments where TMB has been oxidised by various amounts of
153 OH using the Go:PAM unit. Generally, a high OH production, induced either by increased light exposure
154 (two lamps) or elevated ozone concentration, resulted in new particles (e.g. exp 3 and 4) while addition
155 of NO_x reduced or suppressed the particle formation. The results from the kinetic model show that the
156 amount of reacted TMB ranges from 5 – 30 ppb, depending on OH exposure (SI Figure S1). An overview
157 of the oxidation product distribution measured with the CI- APi-TOF-MS for different conditions is

shown in Figure 3 and 4. The compounds were detected as nitrate clusters at $m/z = $ mass$_{compound}$ + 62. The spectra in Figure 3 and 4 show significant ion signals from oxygenated hydrocarbons retaining the 9 carbons from the original TMB with either even H numbers (closed shell) or odd H numbers (open shell) with limited amount of products from fragmentation, i.e. ions with less than nine C. C_9 compounds with an O/C ratio of 6/9 or higher were classified as HOM monomers with the general formula $C_9H_{12-16}O_{6-11}$ in the mass range 280 – 360 m/z. Oxygenated hydrocarbons found in the range 460 – 560 m/z containing 18 C were classified as dimers with chemical formulas $C_{18}H_{24-30}O_{10-16}$. The monomer with the highest intensity detected was $C_9H_{14}O_7$ m/z 296. The highest intensities among the dimers were $C_{18}H_{26}O_{10}$, $C_{18}H_{28}O_{11}$ and $C_{18}H_{28}O_{12}$ at m/z 464, m/z 482 and m/z 498, respectively. In addition to HOM monomers and dimers, nitrogen containing compounds were found as C_9 compounds with one or two N or C_{18} compounds with one N. The nitrogen containing compounds were of the general formulas $C_9H_{12-18}NO_{6-13}$, $C_9H_{12-18}N_2O_{8-15}$ and $C_{18}H_{18-24}NO_{6-10}$. The dominating ON were $C_9H_{13}NO_8$ at m/z 325, $C_9H_{15}NO_{10}$ at m/z 359 and $C_9H_{14}N_2O_{10}$ at m/z 372 respectively. In the experiments where NO$_x$ was added, the formation of ON compounds was increasing with the NO$_x$ concentration. In parallel, the levels of HOM monomers and dimers were reduced with NO$_x$ concentration, where dimers were stronger affected than monomers. Even if the fragmentation products were limited some fragmentation leading to less than 9 carbons could be observed. The most prominent fragments were assigned molecular formulas $C_4H_7NO_7$ at m/z 243, $C_4H_6O_{12}$ at m/z 246, $C_5H_6O_{12}$ at m/z 258 and $C_6H_9NO_7$ at m/z 269. Some compounds with C numbers of 15 and 17 were detected in the range 270 – 560 m/z but their contribution to the total signal was negligible (Figure 3).

Table 1: Experimental conditions for experiments with 30 ppb TMB. Ozone and initial NOx concentration at time 0 are given in ppb and explicitly modelled OH exposure in molecules s cm^{-3}. TMB reacted (Δ TMB) in ppb after a reaction time of 34 s and particle number concentration given in # cm^{-3} after reaching steady state in Go:PAM. RH in all experiments was 38%.

| #	$[O_3]_0$	$[NO_x]_0$	OH exposure	Δ TMB	NO$_x$ /ΔTMB	Particle number	Contribution of top 10 species (%)
1	~19	5	3.5×10^9	5.4	0.9	-	28.6
2	~19	5	7.1×10^9	9.9	0.5	-	29.8
3	~100	3	3.8×10^{10}	26	0.1	60 ± 14	38.6
4	~100	3	2.1×10^{11}	30	0.1	1610 ± 217	35.9
NOx9	~9	82	6.3×10^9	9	9.1	-	52.4
NOx3$_L$	~12	38	7.9×10^9	11	3.5	-	42.3
NOx3$_H$	~100	79	3.1×10^{10}	25	3.2	-	34.2
NOx1	~100	35	9.1×10^{10}	30	1.2	170 ± 50	30.5

The relative contribution of the different compound classes to the total assigned signal are shown in Figure 2. It is apparent that HOM monomers and dimers dominate in the experiments with low NO$_x$. The contribution of the monomers to the total oxidation product signal ranges from 20.7- 42.1% and dimers make 6.8 – 43.3 % of the total, depending on experimental conditions. Dimer contributions are highest at high OH exposure (exp 3 and 4 with estimated OH exposure of 3.8×10^{10} and 2.1×10^{11} molecules s cm^{-3}, respectively) and decrease with increasing NO$_x$. Nitrated compounds dominated the spectra with contributions up to ~75% in the experiments with highest amount of NO$_x$. Surprisingly, some nitrated compounds were also found in the experiments without added NO$_x$ which may stem from background NO contamination (~3-5ppb).
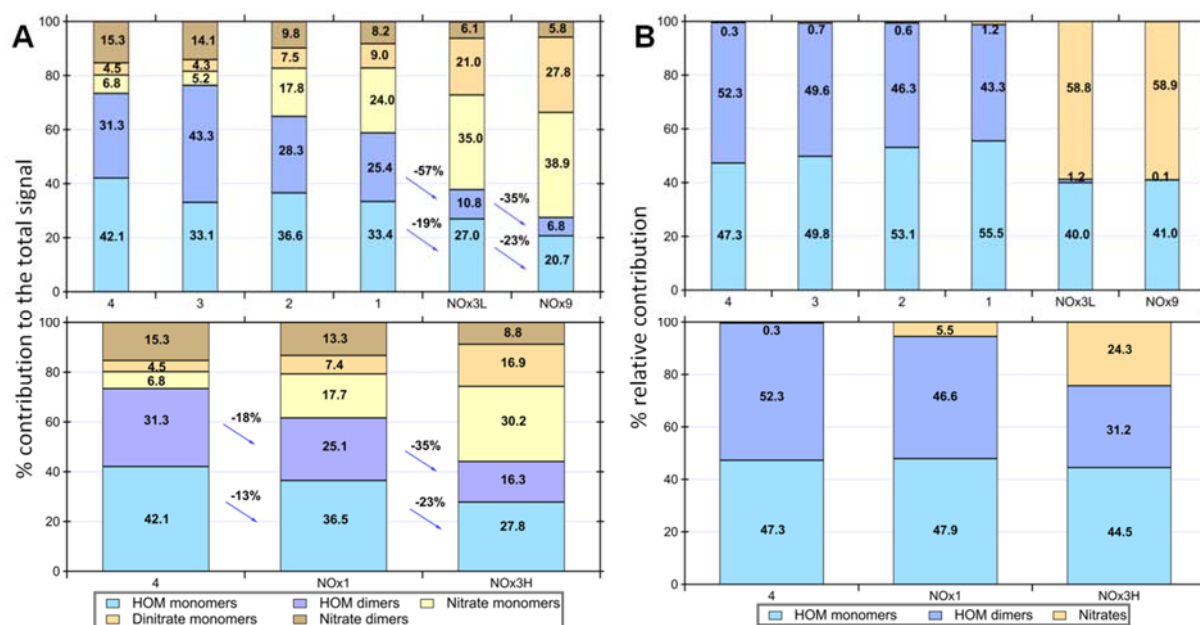
Figure 2: A) Overview of different compound groups to the total explained signal. Top panel illustrates the influence of a decrease of OH exposure (exp 4 - exp 1) and further decrease after adding NO$_x$ in exp NOx3L – exp NOx9. Dimers show a larger relative reduction than monomers with increasing NO$_x$/VOC. Bottom panel shows the influence of increased NO$_x$/VOC on the product distribution. Experiments 4, 3 and NOx1 resulted in particle formation. B) Modelled product distribution shown as lumped categories of nitrated compounds, HOM monomers and dimers and their relative contributions

Recently, Molteni et al. (2018) assigned 17 compounds making up 80% of the total detected signal for HOM oxidation products from the reaction of TMB with OH. Their compound with the highest fraction of the signal (24.2%) was the dimer $C_{18}H_{26}O_8$. This compound was not detected in our study. We did neither detected deprotonated compounds in the mass range 270 – 560 m/z nor HOM monomers with 17 H nor compounds with O/C<0.55 which were found by Molteni et al. (2018). However, we do find 10 of the previously reported 17 monomers and dimers in our spectra. The oxidation product distributions in our experiments are in general term more diverse, i.e. we found more compounds with smaller yields compared to Molteni et al. (2018). In our experiments the highest 20 compounds together explain 46 – 63 % of the total signal with the individual highest oxidation products contributing only between 4.4 and 16%. These differences can be the result of different experimental conditions and set up. In our study the residence time is almost double compared to Molteni et al., leading to the formation of more oxidized compounds, especially more oxidized dimers, which have been reported in this study. In addition we produce OH radicals through irradiation at 254 nm in the full length of the flow reactor enhancing the effects of secondary chemistry. Despite these differences there is a general agreement on the conclusions for the NO$_x$ free conditions with the Molteni et al. study where one rapidly form HOM of very low volatility, that can initiate NPF.
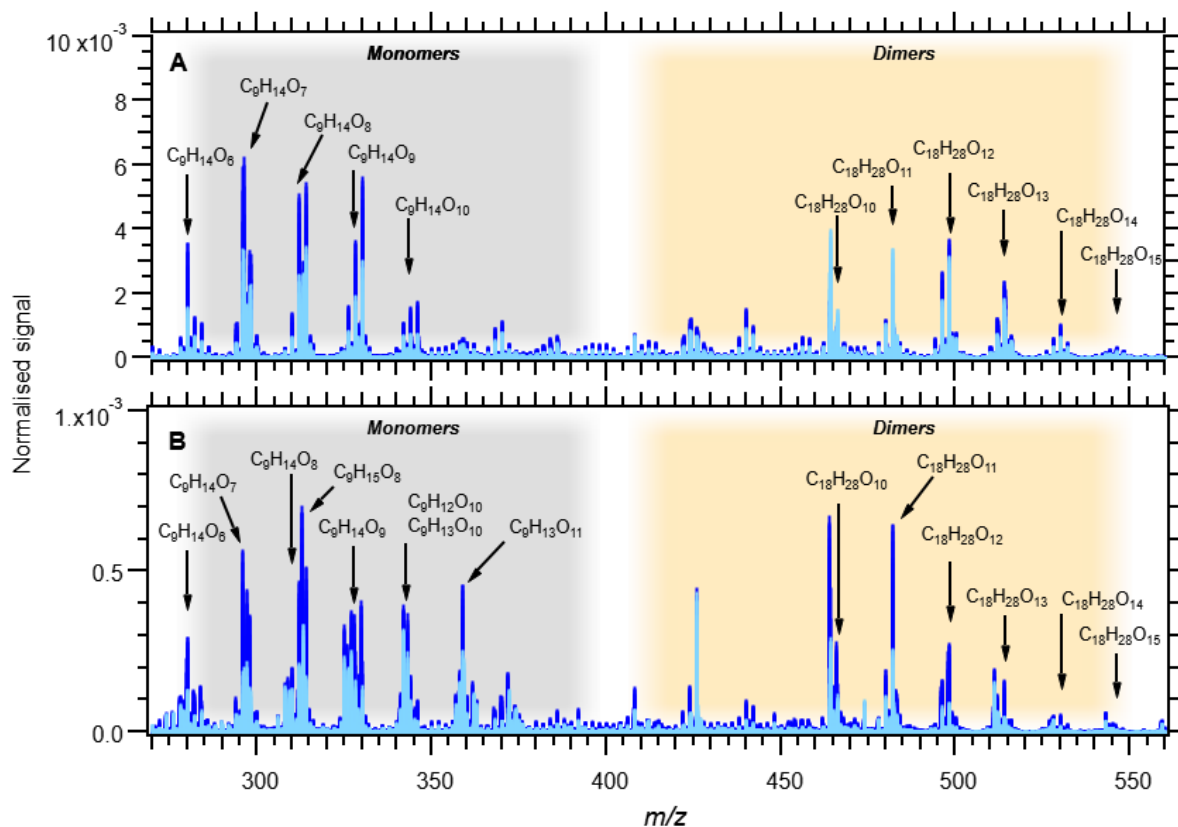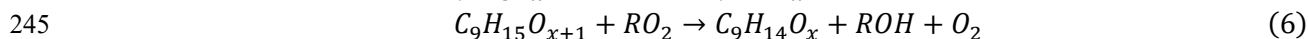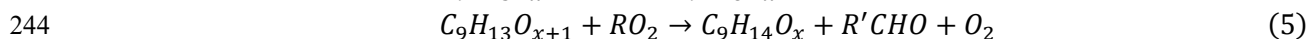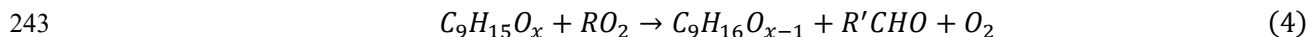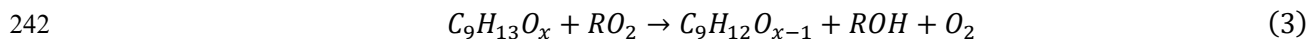
Figure 3: Mass spectra of all experiments without NO$_x$: 1, 2, 3, and 4. Panel A shows experiments 3 (light blue) and 4 (blue) with OH exposure of 2.87×10^{11} and 3.47×10^{11} molecules s cm^{-3} respectively. Panel B shows experiment 1 (light blue) and 2 (blue) with of 3.47×10^{10} and 7.62×10^{10} molecules s cm^{-3} respectively. The signal at m/z 426 is associated with the used mass calibrant PFHA. Note the ten times lower Normalised Signal scale in B.

217 The amount of TMB reacted after 34 s in the experiments ranges from 30 ppb (almost all) in experiment
218 4 to 5 ppb in experiments 1 and NOx9 (comp. Table 1 and Figure S1). The signal intensities of the HOM
219 monomers are increasing with increasing OH exposure. Dimer compounds also increase with increasing
220 OH and reach their highest levels in exp 3, resulting in the highest ratio of dimer to monomer (see Figure
221 2). Faster conversion of TMB will result in higher initial RO$_2$ levels enabling faster RO$_2$ + RO$_2$ (self-)
222 reaction. The concentration profile of RO$_2$ in exp 1 and 2 is lower and more evenly spread out over the
223 length of Go:PAM (Figure S1) and the influence of the RO$_2$ + RO$_2$ reaction will be less in these
224 experiments compared to exp 3 and 4. Enhanced OH exposure does not only affect the monomer/dimer
225 ratio but also the total amount of compounds measured. Observed compounds were 10 times higher in
226 the high OH exposure exp 3, 4, compared to exp 1, 2. This was also valid for the experiments with added
227 NO$_x$ (NOx1 and NOx3$_H$ *vs* NOx3$_L$ and NOx9). Under high OH exposure (exp 4) the major HOM
228 monomer is C$_9$H$_{14}$O$_7$ with a contribution of 5.5 % to the total explained signal, followed by C$_9$H$_{16}$O$_9$
229 and C$_9$H$_{14}$O$_8$, contributing 4.6 and 4.5 % respectively.
230 At the lowest OH exposure (exp 1) the major signals comprise the monomer C$_9$H$_{12}$O$_{10}$ and the dimers
231 C$_{18}$H$_{26}$O$_{10}$ and C$_{18}$H$_{28}$O$_{11}$, contributing 4.4, 4.0 and 3.4 % to the total. These dimer compounds,
232 C$_{18}$H$_{26}$O$_{10}$ and C$_{18}$H$_{28}$O$_{11}$, are the highest signals in exp 2 and 3. Two open shell species were found
233 among the larger signals in exp 1 and 2 (see Figure 3): C$_9$H$_{15}$O$_8$ and C$_9$H$_{15}$O$_7$.
234   The number of H atoms is a characteristic for HOM monomers and dimers. An overview of
235 different oxidation product generations is given in Table 2. We observe HOM monomers with 12-16 H
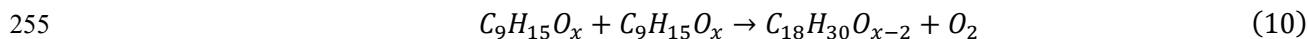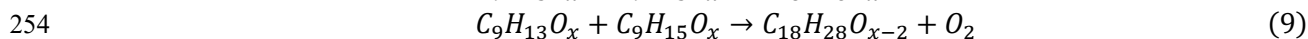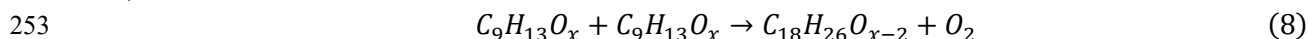
and all compounds with an even number of H are closed shell products. Compounds with an uneven number of H are open shell molecules (radicals). Following the proposed termination scheme by Mentel et al. (2015) compounds with 12 H can be identified as first generation monomers (terminated from $C_9H_{13}O_x$ radicals, reaction 3) and compounds with 16 H as second generation monomers (terminated from $C_9H_{15}O_x$ radicals, reaction 4). $C_9H_{14}O_x$ can be either first or second generation products and originate from either $C_9H_{13}O_x$ or $C_9H_{15}O_x$ (reactions 5 and 6).

$$C_9H_{13}O_x + RO_2 \rightarrow C_9H_{12}O_{x-1} + ROH + O_2 \tag{3}$$
$$C_9H_{15}O_x + RO_2 \rightarrow C_9H_{16}O_{x-1} + R'CHO + O_2 \tag{4}$$
$$C_9H_{13}O_{x+1} + RO_2 \rightarrow C_9H_{14}O_x + R'CHO + O_2 \tag{5}$$
$$C_9H_{15}O_{x+1} + RO_2 \rightarrow C_9H_{14}O_x + ROH + O_2 \tag{6}$$

The RO_2 radicals $C_9H_{13,15}O_x$ can form dimers likely via the reaction

$$HOM - RO_2 + HOM - RO_2 \rightarrow HOM - DIMER + O_2 \tag{7}$$

Such reaction is possible between any HOM-RO₂, first or second generation (and other C_9 peroxy radicals with sufficient high abundance). Two first generation HOM-RO₂ will result in $C_{18}H_{26}O_x$ dimers (reaction 8) while one first and one second generation HOM-RO₂ produce a $C_{18}H_{28}O_x$ (reaction 9) and dimerization of two second generation HOM-RO₂ will result in dimers of the formula $C_{18}H_{30}O_x$ (reaction 10).

$$C_9H_{13}O_x + C_9H_{13}O_x \rightarrow C_{18}H_{26}O_{x-2} + O_2 \tag{8}$$
$$C_9H_{13}O_x + C_9H_{15}O_x \rightarrow C_{18}H_{28}O_{x-2} + O_2 \tag{9}$$
$$C_9H_{15}O_x + C_9H_{15}O_x \rightarrow C_{18}H_{30}O_{x-2} + O_2 \tag{10}$$

A closer examination of the contribution of different HOM generations in Table 2 shows that first generation monomers with 12 H are showing the highest contribution in experiments with low OH exposure (exp 1, 2) while monomers with 14 H gain importance with higher OH exposure. The second generation monomers with 16 H dominate in experiments with the highest OH exposure (exp 3, 4). The dimer population with 28 H has a larger fraction of the total signal at higher OH exposures compared to dimers with 26 H. Dimer population with 30 H is generally lower than other dimers but has the highest fraction in exp 4. The overall dimer fraction of up to 43% in this study (Figure 2) is similar to the dimer fraction of 40% reported by Molteni et al. (2018). However, the relative contributions of monomer and dimer generations differ. We find higher contributions of H_{12} monomers (up to 11%) and a higher contribution of H_{28} dimer (up to 12%) under our experimental conditions. The contribution of H_{14} monomers and H_{26} dimers is significantly less compared to Molteni et al. (2018).

Increasing OH exposure promotes second OH attacks on oxidation products leading to the observed reduction of first generation products ($C_9H_{12}O_x$) as well as increase of second generation products ($C_9H_{14}O_x$ and $C_9H_{16}O_x$). The $C_9H_{14}O_x$ products have mainly characteristics of second generation products, as their contribution is enhanced in the experiments with higher OH exposures (Table S1), in which there is an enhanced possibility for secondary chemistry initiated by reaction of OH with the first generation products. The increased oxidation degree can also explain the formation of dimers ($C_{18}H_{28}O_x$) from first and second generation RO_2 ($C_9H_{13}O_x$ and $C_9H_{15}O_x$) at higher OH exposure and the increase in second generation dimers. Open shell species are observed as first generation RO_2 ($C_9H_{13}O_x$) and have a higher contribution lower at OH exposures. Second generation RO_2 ($C_9H_{15}O_x$) have the highest contribution in exp 3. At the highest OH exposures in exp 4, the contribution of $C_9H_{15}O_x$ radicals, one of the top ten contributors to the signal (Table S1), is reduced, while the contribution of the second generation products ($C_9H_{14}O_x$ and $C_9H_{16}O_x$) and dimers increased.

Table 2: Contribution of oxidation product families to the total signal between 270 – 560 *m/z*

| Compound family	1	2	3	4	NOx9	NOx3$_L$	NOx3$_H$	NOx1
$C_9H_{12}O_x$	11.3	7.8	3.5	5.4	8.5	9.3	5.9	5.4
$C_9H_{13}O_x$	5.7	4.5	3.3	2.1	6.0	7.0	5.6	4.2
$C_9H_{14}O_x$	8.3	10.8	9.9	17.4	4.3	6.6	8.0	13.0
$C_9H_{15}O_x$	5.6	7.2	9.4	4.1	2.4	3.3	4.6	4.7
$C_9H_{16}O_x$	4.8	8.0	7.7	14.5	1.5	2.5	4.8	10.3
$C_{18}H_{26}O_x$	8.5	9.1	8.5	9.3	0.8	2.0	2.7	6.0
$C_{18}H_{28}O_x$	7.1	9.9	9.3	11.0	0.4	1.2	2.6	6.9
$C_{18}H_{30}O_x$	0.7	1.0	2.3	2.6	0.4	0.4	0.9	1.7
$C_9H_{13}NO_x$	6.2	4.7	0.6	0.6	26.8	17.1	10.1	4.8
$C_9H_{15}NO_x$	6.4	5.6	0.7	0.9	3.7	10.3	14.5	8.5
$C_9H_{14}N_2O_x$	2.1	1.7	1.0	1.1	18.7	11.8	7.5	1.9

In this study the contribution of $C_{18}H_{28}O_x$ shows that both first and second generation HOM-RO_2 were dimerising. The kinetics of dimer formation, if produced from RO_2 self-reaction, depends on the square of [HOM-RO_2] and their relative importance will increase with the RO_2 concentration. Increased local RO_2 concentrations (in the first part of Go:PAM) would explain the increase of dimers with increasing OH exposure.

Substantial particle formation was observed in exp 4, under the highest OH exposure. Although the amount of reacted TMB in exp 3 and 4 is similar (26 and 30 ppb respectively), significant particle formation was not observed under the conditions of exp 3. The rate at which new particle formation (nucleation) occurs is related to the chemical composition and concentration of the nucleating species (McGraw and Zhang, 2008). After reaching the critical nucleus, particle growth becomes spontaneous in the presence of condensable vapour. Apparently, the local concentration of nucleating species or condensable vapour was not high enough in exp 3 to yield large numbers of particles, compared to exp 4. According to recent studies (Ehn et al., 2014;Trostl et al., 2016;Mohr et al., 2017;McFiggans et al., 2019) dimers play an important role in new particle formation. Mohr et al. (2017) found decreased levels of gas phase dimers in ambient air during NPF events, which is in line with our observations of lower dimer levels in the presence of particles in exp 4, compared to exp 3. A large enough concentration of low volatility dimers obviously helps forming critical nucleii that then grow by condensation. Note that the newly formed particles will provide an additional sink for dimers and thus reduce their presence as observable gas phase products at the end of the flow reactor.

Influence of NO$_x$

In the experiments NOx1, NOx3$_H$, NOx3$_L$ and NOx9, the NO$_x$ levels were increased (Table 1). As already has been described NO$_x$ was introduced to the Go:PAM as NO. After the addition of ozone, the ozone concentration decreases from 100 ppb to ~80 ppb at the experiment with lower NO$_x$ levels and to ~50 ppb at the experiment with higher NO$_x$ levels, as it reacts with NO producing NO$_2$. For both high and low NO$_x$ conditions there is NO left after the initial reaction with ozone (see grey areas of Figure S3). The presence of NO$_x$ gave nitrogen containing C_9 compounds with one or two N atoms and C_{18} compounds with only one N atom, in addition to HOM monomers and HOM dimers. These compounds are expected to be nitrates or peroxy nitrates, as it is highly unlikely to form nitro-aromatic compounds from TMB (Sato et al., 2012). N-containing compounds were the dominating species in experiments with NO$_x$ (see Figure 2), except for the experiment NOx1 with the smallest amount of NO$_x$

added and a high OH exposure (NOx1). The amount of nitrated compounds increased with the amount of added NO_x at the expense of HOM monomers and HOM dimers as illustrated by the arrows in Figure 2. The effect of the added NO_x is attenuated at higher OH exposure. E.g., the nitrated monomers are reduced from 35.0 and 38.9% at low OH exposure down to 17.7 and 30.2% at high OH exposure. Under elevated NO_x conditions nitrated species were found among the 10 compounds with the highest contribution to the respective total signal, (see the top-ten lists Table S1 and Figure 4).
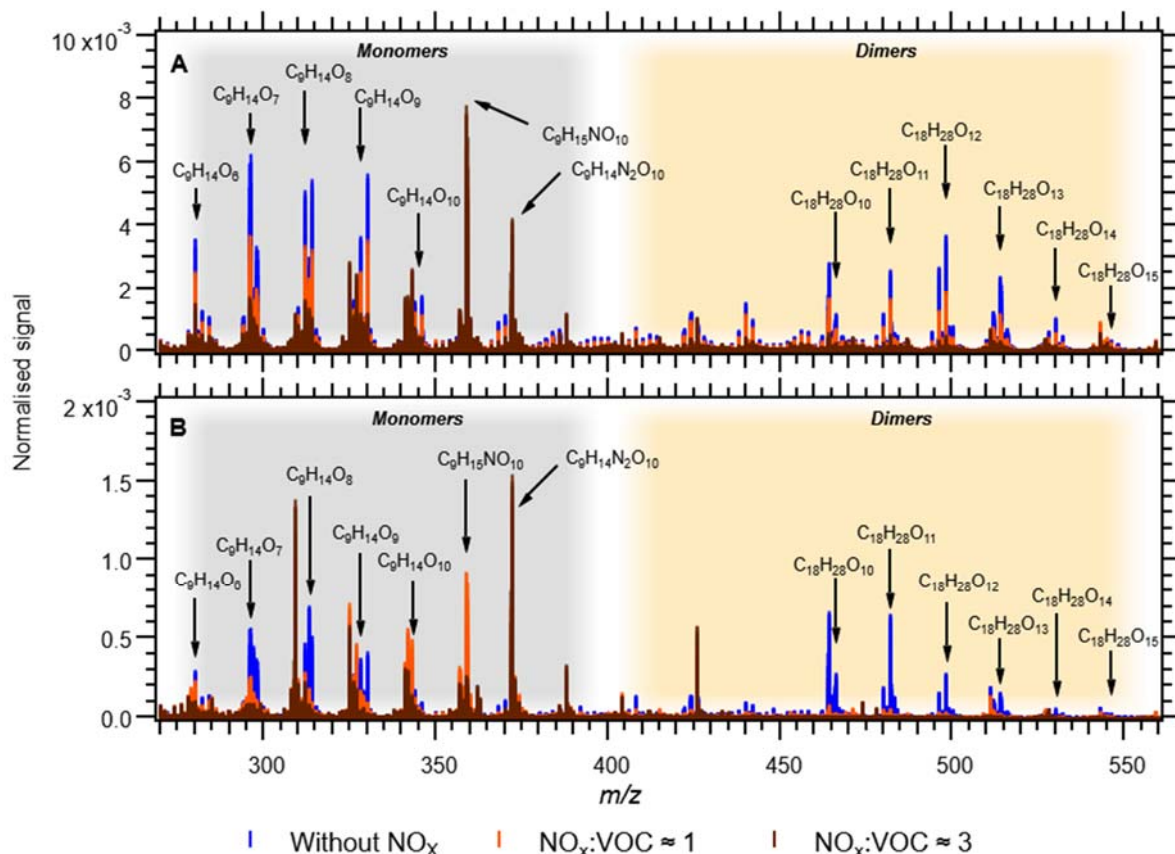
Figure 4: Comparison of mass spectra of HOM and nitrates. Panel A shows experiment 4 (blue), NOx1 (orange) and experiment $NOx3_H$ (brown). Panel B shows experiments 2 (blue), $NOx3_L$ (orange) and NOx9 (brown).

For the two experiments with low OH exposure where the nitrated species dominated, seven out of the top ten species were nitrated with the highest signal arising from the di-nitrated compound ($C_9H_{14}N_2O_{10}$). In these two experiments the top-ten compounds contributed the most to the observed signal (42.3 and 52.4%); most likely owing to the high fraction of nitrated species acting as radical chain termination products. Under highest NOx conditions, the high OH exposure experiment ($NOx3_H$) has six nitrated compounds in the top-ten list with the di-nitrated $C_9H_{14}N_2O_{10}$ on the second rank. In experiment NOx1 only one nitrated species ($C_9H_{15}NO_{10}$) is found in the top-ten list despite the elevated NOx conditions.

Dimer formation is drastically reduced in the presence of elevated NO_x. The NO_x effect on NPF was clear and high NO_x/ΔTMB supresses NPF from TMB oxidation, a trend that was also observed by Wildt et al. (2014) and Lehtipalo et al. (2018) for NPF from monoterpene oxidation. Whenever the products were dominated by ON ($NOx3_L$, NOx9 and $NOx3_H$) particle formation was not observed. Reduced particle formation was observed in NOx1 compared to exp 1 which had a higher contribution of HOM. Owing to the importance of dimers for NPF, as reported by Lehtipalo et al. (2018), we suggest

338   that the reaction of $RO_2 + NO$ resulting in ON is responsible for the observed reduced particle formation,
339   because it competes with the dimer formation from $RO_2 + RO_2$, This reaction is also reducing the
340   contribution of HOM monomers and dimers with increasing $NO_x/\Delta TMB$ and decreasing OH exposure
341   from a total of 61% in exp NOx1 (OH exposure=9.1×10^{10} molecules s cm^{-3}) to 27.5% in NOx9 (OH
342   exposure=6.3×10^{9} molecules s cm^{-3}). The reaction $RO_2 + NO$ reduce the amount of HOM monomers
343   and dimers in competing with autoxidation and termination by RO_2+RO_2 or RO_2+HO_2. The yield of ON
344   from $NO+RO_2$ might be significant (e.g. up to 0.3) based on the measurable increase of ON and the
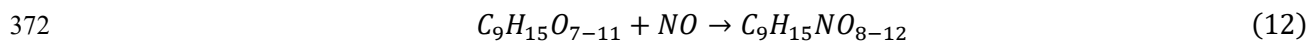345   decrease of NO_x in the system (Figure S3).
346   The contribution of HOM monomer generations follows the general trend observed in
347   experiments without NO_x. The first generation HOM have higher contribution at low OH exposures in
348     $NOx3_L$ and $NOx9$ and the contribution of second generation HOM is higher the higher the OH exposure
349   is. Similarly, the contribution of $C_9H_{14}O_x$ is increasing with increasing OH exposure. Analogously to the
350   families of HOM, different families of nitrates can be defined. Table 2 gives an overview of the nitrate
351   families and how they contribute to the total signal in the experiments. At lowest OH exposures we find
352   the highest contributions of first generation nitrates ($C_9H_{13}NO_x$) as well as di-nitrates ($C_9H_{14}N_2O_x$). The
353   contribution of second generation nitrates ($C_9H_{15}NO_x$) is increasing with increasing OH exposure and is
354   highest in $NOx3_H$.
355   For the formation of observed first generation nitrates $C_9H_{13}NO_{6-12}$ ($C_9H_{13}NO_x$ in Table 2) we
356   propose the reaction of a first generation (HOM-)RO_2 with NO following the pathway:

$$C_9H_{13}O_{5-11} + NO \rightarrow C_9H_{13}NO_{6-12} \tag{11}$$
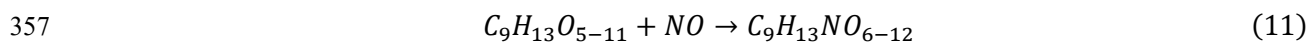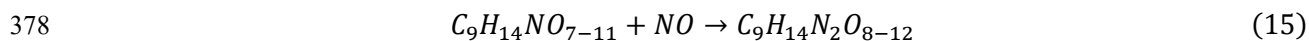
358 The precursor $C_9H_{13}O_5$ is formed after one autoxidation step and its termination reaction with NO results
359 in $C_9H_{13}NO_6$ which has only minor contribution. $C_9H_{13}NO_{7\&8}$, with higher contribution in exp $NOx3_L$
360 and $NOx9$ can be formed from the radicals $C_9H_{13}O_6$ and $C_9H_{13}O_7$ respectively. The even oxygen number
361 in $C_9H_{13}O_6$ indicates that the compound should have undergone a transformation to RO (via reaction
362 with RO_2 or NO) and subsequent H-shift and further O_2 addition (Vereecken and Peeters, 2010;Mentel
363 et al., 2015). A proposed detailed reaction mechanism is depicted in the Figure 5.
364 Second generation nitrates ($C_9H_{15}NO_{8-12}$) can be formed after an additional OH attack (and introduction
365 of an additional H) on a first generation (HOM) monomer, which explains the increase of these
366 compounds with increasing OH exposure. The termination of the RO_2 radical chain with NO (reaction
367 12) will then lead to the formation of the second generation nitrate. The formation of RO_2 precursor
368 species with 7-8 O numbers, i.e. $C_9H_{15}O_{7-8}$ likely stem from compounds terminated earlier in the radical
369 chain process ($C_9H_{14}O_{4-5}$), which do not fall in the typical HOM class ($O{:}C \geq 6{:}9$). The reaction of a first
370 generation nitrate with OH, followed by autoxidation could also possibly produce $C_9H_{15}NO_{8-12}$ by
371 terminating via peroxy (reaction 13) or hydroperoxy pathway (reaction 14).

$$C_9H_{15}O_{7-11} + NO \rightarrow C_9H_{15}NO_{8-12} \tag{12}$$
$$C_9H_{14}NO_{9-13} + RO_2 \rightarrow C_9H_{15}NO_{8-12} + Carbonyl\ products + O_2 \tag{13}$$
$$C_9H_{14}NO_{8-12} + HO_2 \rightarrow C_9H_{15}NO_{8-12} + O_2 \tag{14}$$

375 For the formation of the most abundant di-nitrates of the formula $C_9H_{14}N_2O_{8-12}$ (reaction 15), OH has to
376 attack a nitrated compound $C_9H_{13}NO_{6-10}$ and the RO_2 radical chain has to be terminated with NO (Figure
377 5).

$$C_9H_{14}NO_{7-11} + NO \rightarrow C_9H_{14}N_2O_{8-12} \tag{15}$$

379 The precursor species $C_9H_{14}NO_7$ would be in this case formed from the OH attack on the smallest
380 possible nitrate $C_9H_{13}NO_4$ (formed after one autoxidation step and NO termination).

381 It should be noted that the formation of peroxy nitrates via the reaction $RO_2 + NO_2 \rightarrow RO_2NO_2$ with
382 alkyl and acyl-RO_2 (PAN-like) cannot be ruled out as a potential formation mechanisms of nitrates.
383 The volatility of the produced ON seems to be too high (compared to dimers) to initiate NPF at the
384 present concentrations as seen from the reduction in particle formation potential from exp 4 (HOM
385 dominated, particle formation) to NOx1 (reduction in HOM and increase in ON, reduced particle
386 formation) and NOx3$_H$ (ON dominated, no particle formation).
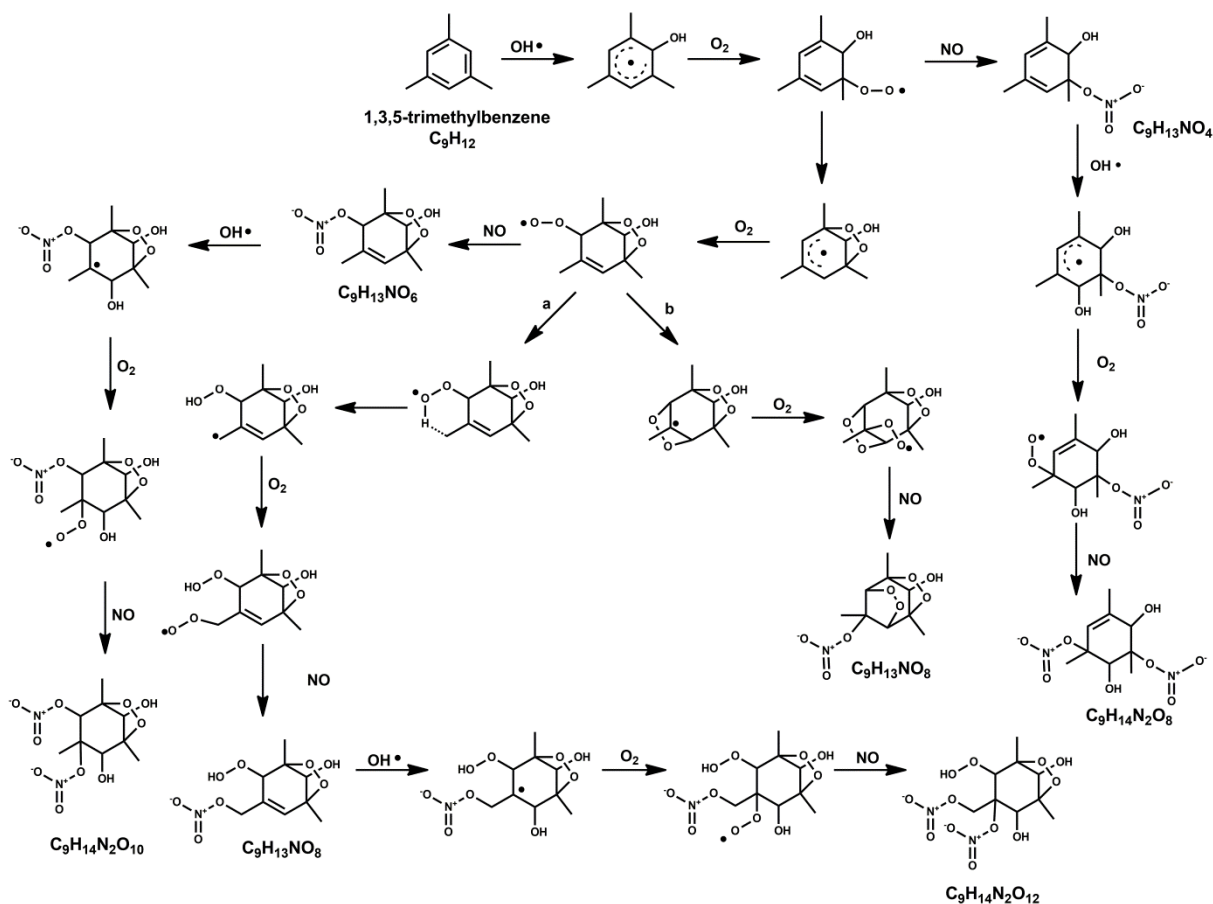
387
388 **Figure 5: The proposed radical reaction mechanism for the formation of some of the mono- and**
389 **di-nitrates from TMB mentioned in this study. Two separate mechanisms were suggested for the**
390 **species with the formula $C_9H_{13}NO_8$, which formation pathways are based on (a) (Wang et al., 2017)**
391 **and (b) (Molteni et al., 2018).**

392   Figure 2B shows the results for the evolution of HOM monomer, HOM Dimers and organic
393 nitrates (ON) as calculated using the kinetic model described in detailed in SI. The model used has a
394 very simplified scheme for TMB oxidation and subsequent RO_2 chemistry. We implemented a few rate
395 coefficients suggested in the literature in order to demonstrate how those compare with our experimental
396 results. Rate coefficients for RO_2 termination reactions from MCM in combination with rate coefficients
397 of dimer formation by Berndt et al. (2018) (case 1 and 2 in SI Table S2) led to an overestimation of
398 dimer compounds. Better representation of the observations were achieved by applying a) the rate
399 coefficients proposed by (Zhao et al., 2018) for dimer formation (2.0×10^{-12} cm^{3}molecules^{-1} s^{-1}) and
400 1.0×10^{-12} cm^3 molecules^{-1} s^{-1} for termination and RO formation with branching ratios of 0.4 and 0.6,
401 respectively; b) the rate coefficient (1.0×10^{-11} cm^{3}molecules^{-1} s^{-1}) from Berndt et al. (2018) for HOMRO$_2$
402 + NO with a branching ratio of 0.3 for ON formation (reaction 56 in Table S2).
403   In Figure 2B, the calculated HOM dimer contribution are the sum of medium (produced from
404 HOM-RO_2+RO_2), and highly oxidised dimers (produced from HOM-RO_2 + HOM-RO_2) while the ON

405 includes both organic nitrates (produced from HOM-RO$_2$+NO) and peroxy nitrates (produced from
406 HOM-RO$_2$+NO$_2$). The increased production of monomers calculated for exp 1 and 2 is in agreement
407 with experimental results, where we observed a slightly larger contribution from monomers compared
408 to dimers. Calculated concentrations for dimers are similar in exp 3 and higher in exp 4, compared to
409 monomers. Secondary chemistry (reaction of OH with the products and possible formation of a second
410 generation of HOM or nitrates) was not taken into consideration in the model. For the experiment with
411 NO$_x$ (Figure 2B) the modeled product distribution follows the general trend of monomer, dimer and
412 nitrate that we observe in the exp NOx3$_L$ and NOx9 with a general higher nitrate production compared
413 to monomers and dimers. For the NO$_x$ experiments with high initial ozone, the model can reproduce the
414 higher HOM monomer and dimer levels in NOx1 but slightly overestimates the contribution of dimers.
415 Particle formation was observed in NOx1 which might explain the overestimation owing to missing
416 condensation sink in the model. Modelling NOx3$_H$ gives an overestimation of monomers and dimers.
417 In NOx3$_H$ modelled dimers start forming after ~15 sec. Almost all NO is converted to ON or NO$_2$ at this
418 point and the reaction HOM-RO$_2$+NO does not produce additional ON and the modelled levels of ON
419 reach a plateau while contribution of HOM dimers can increase. For exp NOx1 and NOx3$_H$ the model
420 is in better agreement with the measurements if only the HOM - dimer formation (from HOM-
421 RO$_2$+HOM-RO$_2$) is taken into account, i.e. highly oxidized dimers excluding medium oxidized dimer
422 (from HOM-RO$_2$ + RO$_2$). Generally, the simplified model was able to support our analysis of the TMB
423 chemistry as described above. Furthermore, it gave some support to the recently suggested mechanisms
424 included in case 3 (e.g. (Zhao et al., 2018))
425

426 **4   Atmospheric implication and Conclusion**

427   We have measured the formation of HOM monomers and dimers from OH initiated oxidation
428 of TMB. The experiments with highest OH exposures lead to particle formation when NO$_x$ was not
429 added. With increasing OH exposure and increased likelihood of a second OH attack, we observe a
430 higher contribution from second generation oxidation products and dimers in general. The latter is
431 attributed to the increased RO$_2$ concentrations from the increased/fast TMB consumption by OH. The
432 observed products in this study match what would be expected as termination products from previously
433 proposed reaction mechanisms for HOM formation.
434   The addition of NO$_x$ to simulate urban condition leads to the formation of ON in addition to
435 HOM and a reduction in particle formation potential. We observe that the formation of ON is increasing
436 with increasing NO$_x$/ΔTMB, mostly at the expense of dimers. The presence of ONs, formed at the
437 expense of dimers, can explain the decreased tendency for particle formation. We therefore suggest that
438 the reaction HOM-RO$_2$+NO competes with HOM-RO$_2$ self-reaction yielding primarily a reduction in
439 dimer formation, which is responsible for the reduction in particle formation. The experimental designed
440 using the Go:PAM with concentrations of HO$_x$ (and RO$_x$) higher than ambient would attenuate the
441 influence of added NO$_x$. This will further emphasis the implication of our findings and most likely the
442 NO$_x$ effect would be even more important in the urban atmosphere.
443   According to studies by (Molteni et al., 2018) and (Wang et al., 2017) HOM formation from
444 AVOCs was observed and consequently AVOC-HOM were suggested as potential contributors to
445 observed NPF in urban atmospheres. In our study, under NO$_x$ free conditions, we found several of
446 previous identified HOM even if we did not fully agree with the identity and relative importance of all
447 HOM. However, the oxidation in polluted environments will happen under elevated NO$_x$ levels and, as
448 has been shown here this can lead to formation of ON instead of HOM and subsequently a reduction in
449 NPF potential. We conclude that for interpretation of NPF from aromatics in urban areas care should be

450 taken and the OH exposure, NO_x levels and RO_2 concentrations need to be considered in details since
451 they will largely determine if the HOM-RO_2+NO can compete with reactions yielding HOM, and
452 especially HOM dimers.

453
454

457 *Competing Interests*: The authors declare that they have no conflict of interest.

458 *Author contribution*: J.H., E.T. T.M. and M.H. designed the experiments. J.H and E.T performed the
459 experiments and data analysis. E.T. performed the modelling. C.M.S. designed the chemical
460 mechanisms. E.T., J.H. and M.H. wrote the paper. All authors commented on the paper and were
461 involved in the scientific interpretation and discussion.

465

5. References:

468 Atkinson, R., Baulch, D. L., Cox, R. A., Hampson, R. F., Kerr, J. A., and Troe, J.: Evaluated Kinetic and Photochemical Data
469   for Atmospheric Chemistry Supplement-Iv - Iupac Subcommittee on Gas Kinetic Data Evaluation for Atmospheric
470   Chemistry, J Phys Chem Ref Data, 21, 1125-1568, Doi 10.1063/1.555918, 1992.
471 Berndt, T., Richters, S., Jokinen, T., Hyttinen, N., Kurten, T., Otkjaer, R. V., Kjaergaard, H. G., Stratmann, F., Herrmann, H.,
472   Sipila, M., Kulmala, M., and Ehn, M.: Hydroxyl radical-induced formation of highly oxidized organic compounds, Nat
473   Commun, 7, 13677, 10.1038/ncomms13677, 2016.
474 Bianchi, F., Trostl, J., Junninen, H., Frege, C., Henne, S., Hoyle, C. R., Molteni, U., Herrmann, E., Adamov, A., Bukowiecki,
475   N., Chen, X., Duplissy, J., Gysel, M., Hutterli, M., Kangasluoma, J., Kontkanen, J., Kurten, A., Manninen, H. E., Munch,
476   S., Perakyla, O., Petaja, T., Rondo, L., Williamson, C., Weingartner, E., Curtius, J., Worsnop, D. R., Kulmala, M.,
477   Dommen, J., and Baltensperger, U.: New particle formation in the free troposphere: A question of chemistry and timing,
478   Science, 352, 1109-1112, 10.1126/science.aad5456, 2016.
479 Bianchi, F., Garmash, O., He, X., Yan, C., Iyer, S., Rosendahl, I., Xu, Z., Rissanen, M. P., Riva, M., Taipale, R., Sarnela, N.,
480   Petäjä, T., Worsnop, D. R., Kulmala, M., Ehn, M., and Junninen, H.: The role of highly oxygenated molecules (HOMs)
481   in determining the composition of ambient ions in the boreal forest, Atmos Chem Phys, 17, 13819-13831, 10.5194/acp-
482   17-13819-2017, 2017.
483 Bianchi, F., Kurten, T., Riva, M., Mohr, C., Rissanen, M. P., Roldin, P., Berndt, T., Crounse, J. D., Wennberg, P. O., Mentel,
484   T. F., Wildt, J., Junninen, H., Jokinen, T., Kulmala, M., Worsnop, D. R., Thornton, J. A., Donahue, N., Kjaergaard, H.
485   G., and Ehn, M.: Highly Oxygenated Organic Molecules (HOM) from Gas-Phase Autoxidation Involving Peroxy
486   Radicals: A Key Contributor to Atmospheric Aerosol, Chem Rev, 119, 3472-3509, 10.1021/acs.chemrev.8b00395, 2019.
487 Chan, C. K., and Yao, X.: Air pollution in mega cities in China, Atmos Environ, 42, 1-42, 10.1016/j.atmosenv.2007.09.003,
488   2008.
489 Crounse, J. D., Nielsen, L. B., Jorgensen, S., Kjaergaard, H. G., and Wennberg, P. O.: Autoxidation of Organic Compounds in
490   the Atmosphere, J Phys Chem Lett, 4, 3513-3520, 10.1021/jz4019207, 2013.
491 Donahue, N. M., Kroll, J. H., Pandis, S. N., and Robinson, A. L.: A two-dimensional volatility basis set – Part 2: Diagnostics
492   of organic-aerosol evolution, Atmos. Chem. Phys., 12, 615-634, 10.5194/acp-12-615-2012, 2012.
493 Ehn, M., Kleist, E., Junninen, H., Petäjä, T., Lönn, G., Schobesberger, S., Dal Maso, M., Trimborn, A., Kulmala, M., Worsnop,
494   D. R., Wahner, A., Wildt, J., and Mentel, T. F.: Gas phase formation of extremely oxidized pinene reaction products in
495   chamber and ambient air, Atmos Chem Phys, 12, 5113-5127, 10.5194/acp-12-5113-2012, 2012.
496 Ehn, M., Thornton, J. A., Kleist, E., Sipila, M., Junninen, H., Pullinen, I., Springer, M., Rubach, F., Tillmann, R., Lee, B.,
497   Lopez-Hilfiker, F., Andres, S., Acir, I.-H., Rissanen, M., Jokinen, T., Schobesberger, S., Kangasluoma, J., Kontkanen,
498   J., Nieminen, T., Kurten, T., Nielsen, L. B., Jorgensen, S., Kjaergaard, H. G., Canagaratna, M., Maso, M. D., Berndt, T.,
499   Petaja, T., Wahner, A., Kerminen, V.-M., Kulmala, M., Worsnop, D. R., Wildt, J., and Mentel, T. F.: A large source of
500   low-volatility secondary organic aerosol, Nature, 506, 476-479, 10.1038/nature13032, 2014.
501 Eisele, F. L., and Tanner, D. J.: Measurement of the gas phase concentration of H2SO4and methane sulfonic acid and estimates
502   of H2SO4production and loss in the atmosphere, Journal of Geophysical Research: Atmospheres, 98, 9001-9010,
503   10.1029/93jd00031, 1993.
504 Finlayson-Pitts, B. a. P., J.: Chemistry of the Upper and Lower Atmosphere, 1999.
505 Gentner, D. R., Jathar, S. H., Gordon, T. D., Bahreini, R., Day, D. A., El Haddad, I., Hayes, P. L., Pieber, S. M., Platt, S. M.,
506   de Gouw, J., Goldstein, A. H., Harley, R. A., Jimenez, J. L., Prevot, A. S. H., and Robinson, A. L.: Review of Urban

507 Secondary Organic Aerosol Formation from Gasoline and Diesel Motor Vehicle Emissions, Environmental science &
508 technology, 51, 1074-1093, 10.1021/acs.est.6b04509, 2017.
509 Guo, S., Hu, M., Zamora, M. L., Peng, J., Shang, D., Zheng, J., Du, Z., Wu, Z., Shao, M., Zeng, L., Molina, M. J., and Zhang,
510 R.: Elucidating severe urban haze formation in China, Proc Natl Acad Sci U S A, 111, 17373-17378,
511 10.1073/pnas.1419604111, 2014.
512 Hallquist, M., Wenger, J. C., Baltensperger, U., Rudich, Y., Simpson, D., Claeys, M., Dommen, J., Donahue, N. M., George,
513 C., Goldstein, A. H., Hamilton, J. F., Herrmann, H., Hoffmann, T., Iinuma, Y., Jang, M., Jenkin, M. E., Jimenez, J. L.,
514 Kiendler-Scharr, A., Maenhaut, W., McFiggans, G., Mentel, T. F., Monod, A., Prevot, A. S. H., Seinfeld, J. H., Surratt,
515 J. D., Szmigielski, R., and Wildt, J.: The formation, properties and impact of secondary organic aerosol: current and
516 emerging issues, Atmos. Chem. Phys., 9, 5155-5236, 2009.
517 Hallquist, M., Munthe, J., Hu, M., Wang, T., Chan, C. K., Gao, J., Boman, J., Guo, S., Hallquist, A. M., Mellqvist, J.,
518 Moldanova, J., Pathak, R. K., Pettersson, J. B. C., Pleijel, H., Simpson, D., and Thynell, M.: Photochemical smog in
519 China: scientific challenges and implications for air-quality policies, National Science Review, 3, 401-403,
520 10.1093/nsr/nww080, 2016.
521 Hu, M., Guo, S., Peng, J.-f., and Wu, Z.-j.: Insight into characteristics and sources of PM2.5in the Beijing–Tianjin–Hebei
522 region, China, National Science Review, 2, 257-258, 10.1093/nsr/nwv003, 2015.
523 Huang, M., Lin, Y., Huang, X., Liu, X., Guo, X., Hu, C., Zhao, W., Gu, X., Fang, L., and Zhang, W.: Experimental study of
524 particulate products for aging of 1,3,5–trimethylbenzene secondary organic aerosol, Atmos Pollut Res, 6, 209-219,
525 10.5094/apr.2015.025, 2015.
526 Intergovernmental Panel on Climate, C.: Climate Change 2013 - The Physical Science Basis, Cambridge University Press,
527 Cambridge, United Kingdom and New York, NY, USA, 1535 pp., 2014.
528 Jokinen, T., Sipila, M., Junninen, H., Ehn, M., Lonn, G., Hakala, J., Petaja, T., Mauldin, R. L., Kulmala, M., and Worsnop, D.
529 R.: Atmospheric sulphuric acid and neutral cluster measurements using CI-APi-TOF, Atmos. Chem. Phys., 12, 4117-
530 4125, 10.5194/acp-12-4117-2012, 2012.
531 Jokinen, T., Sipila, M., Richters, S., Kerminen, V. M., Paasonen, P., Stratmann, F., Worsnop, D., Kulmala, M., Ehn, M.,
532 Herrmann, H., and Berndt, T.: Rapid autoxidation forms highly oxidized RO2 radicals in the atmosphere, Angewandte
533 Chemie (International ed. in English), 53, 14596-14600, 10.1002/anie.201408566, 2014.
534 Jokinen, T., Berndt, T., Makkonen, R., Kerminen, V. M., Junninen, H., Paasonen, P., Stratmann, F., Herrmann, H., Guenther,
535 A. B., Worsnop, D. R., Kulmala, M., Ehn, M., and Sipila, M.: Production of extremely low volatile organic compounds
536 from biogenic emissions: Measured yields and atmospheric implications, Proc. Natl. Acad. Sci. U.S.A, 112, 7123-7128,
537 10.1073/pnas.1423977112, 2015.
538 Junninen, H., Ehn, M., Petaja, T., Luosujarvi, L., Kotiaho, T., Kostiainen, R., Rohner, U., Gonin, M., Fuhrer, K., Kulmala, M.,
539 and Worsnop, D. R.: A high-resolution mass spectrometer to measure atmospheric ion composition, Atmospheric
540 Measurement Techniques, 3, 1039-1053, 10.5194/amt-3-1039-2010, 2010.
541 Kang, E., Root, M. J., Toohey, D. W., and Brune, W. H.: Introducing the concept of Potential Aerosol Mass (PAM), Atmos.
542 Chem. Phys., 7, 5727-5744, DOI 10.5194/acp-7-5727-2007, 2007.
543 Kirkby, J., Duplissy, J., Sengupta, K., Frege, C., Gordon, H., Williamson, C., Heinritzi, M., Simon, M., Yan, C., Almeida, J.,
544 Trostl, J., Nieminen, T., Ortega, I. K., Wagner, R., Adamov, A., Amorim, A., Bernhammer, A. K., Bianchi, F.,
545 Breitenlechner, M., Brilke, S., Chen, X., Craven, J., Dias, A., Ehrhart, S., Flagan, R. C., Franchin, A., Fuchs, C., Guida,
546 R., Hakala, J., Hoyle, C. R., Jokinen, T., Junninen, H., Kangasluoma, J., Kim, J., Krapf, M., Kurten, A., Laaksonen, A.,
547 Lehtipalo, K., Makhmutov, V., Mathot, S., Molteni, U., Onnela, A., Perakyla, O., Piel, F., Petaja, T., Praplan, A. P.,
548 Pringle, K., Rap, A., Richards, N. A., Riipinen, I., Rissanen, M. P., Rondo, L., Sarnela, N., Schobesberger, S., Scott, C.
549 E., Seinfeld, J. H., Sipila, M., Steiner, G., Stozhkov, Y., Stratmann, F., Tome, A., Virtanen, A., Vogel, A. L., Wagner, A.
550 C., Wagner, P. E., Weingartner, E., Wimmer, D., Winkler, P. M., Ye, P., Zhang, X., Hansel, A., Dommen, J., Donahue,
551 N. M., Worsnop, D. R., Baltensperger, U., Kulmala, M., Carslaw, K. S., and Curtius, J.: Ion-induced nucleation of pure
552 biogenic particles, Nature, 533, 521-526, 10.1038/nature17953, 2016.
553 Kristensen, K., Watne, Å. K., Hammes, J., Lutz, A., Petäjä, T., Hallquist, M., Bilde, M., and Glasius, M.: High-Molecular
554 Weight Dimer Esters Are Major Products in Aerosols from α-Pinene Ozonolysis and the Boreal Forest, Environmental
555 Science & Technology Letters, 3, 280-285, 10.1021/acs.estlett.6b00152, 2016.
556 Kurtén, T., Tiusanen, K., Roldin, P., Rissanen, M., Luy, J.-N., Boy, M., Ehn, M., and Donahue, N.: α-Pinene Autoxidation
557 Products May Not Have Extremely Low Saturation Vapor Pressures Despite High O:C Ratios, The Journal of Physical
558 Chemistry A, 120, 2569-2582, 10.1021/acs.jpca.6b02196, 2016.
559 Lee, B. H., Mohr, C., Lopez-Hilfiker, F. D., Lutz, A., Hallquist, M., Lee, L., Romer, P., Cohen, R. C., Iyer, S., Kurtén, T., Hu,
560 W., Day, D. A., Campuzano-Jost, P., Jimenez, J. L., Xu, L., Ng, N. L., Guo, H., Weber, R. J., Wild, R. J., Brown, S. S.,
561 Koss, A., de Gouw, J., Olson, K., Goldstein, A. H., Seco, R., Kim, S., McAvey, K., Shepson, P. B., Starn, T., Baumann,
562 K., Edgerton, E. S., Liu, J., Shilling, J. E., Miller, D. O., Brune, W., Schobesberger, S., D'Ambro, E. L., and Thornton, J.
563 A.: Highly functionalized organic nitrates in the southeast United States: Contribution to secondary organic aerosol and
564 reactive nitrogen budgets, Proceedings of the National Academy of Sciences, 113, 1516-1521,
565 10.1073/pnas.1508108113, 2016.
566 McFiggans, G., Mentel, T. F., Wildt, J., Pullinen, I., Kang, S., Kleist, E., Schmitt, S., Springer, M., Tillmann, R., Wu, C., Zhao,
567 D., Hallquist, M., Faxon, C., Le Breton, M., Hallquist, A. M., Simpson, D., Bergstrom, R., Jenkin, M. E., Ehn, M.,
568 Thornton, J. A., Alfarra, M. R., Bannan, T. J., Percival, C. J., Priestley, M., Topping, D., and Kiendler-Scharr, A.:
569 Secondary organic aerosol reduced by mixture of atmospheric vapours, Nature, 565, 587-593, 10.1038/s41586-018-0871-
570 y, 2019.
571 McGraw, R., and Zhang, R.: Multivariate analysis of homogeneous nucleation rate measurements. Nucleation in the p-toluic
572 acid/sulfuric acid/water system, The Journal of chemical physics, 128, 064508, 10.1063/1.2830030, 2008.

15

573 Mentel, T. F., Springer, M., Ehn, M., Kleist, E., Pullinen, I., Kurtén, T., Rissanen, M., Wahner, A., and Wildt, J.: Formation of
574   highly oxidized multifunctional compounds: autoxidation of peroxy radicals formed in the ozonolysis of alkenes –
575   deduced from structure–product relationships, Atmos. Chem. Phys., 15, 6745-6765, 10.5194/acp-15-6745-2015, 2015.
576 Mohr, C., Lopez-Hilfiker, F. D., Yli-Juuti, T., Heitto, A., Lutz, A., Hallquist, M., D'Ambro, E. L., Rissanen, M. P., Hao, L. Q.,
577   Schobesberger, S., Kulmala, M., Mauldin, R. L., Makkonen, U., Sipila, M., Petaja, T., and Thornton, J. A.: Ambient
578   observations of dimers from terpene oxidation in the gas phase: Implications for new particle formation and growth,
579   Geophys Res Lett, 44, 2958-2966, 10.1002/2017gl072718, 2017.
580 Molteni, U., Bianchi, F., Klein, F., El Haddad, I., Frege, C., Rossi, M. J., Dommen, J., and Baltensperger, U.: Formation of
581   highly oxygenated organic molecules from aromatic compounds, Atmospheric Chemistry and Physics, 18, 1909-1921,
582   10.5194/acp-18-1909-2018, 2018.
583 Paulsen, D., Dommen, J., Kalberer, M., Prevot, A. S., Richter, R., Sax, M., Steinbacher, M., Weingartner, E., and Baltensperger,
584   U.: Secondary organic aerosol formation by irradiation of 1,3,5-trimethylbenzene-NOx-H2O in a new reaction chamber
585   for atmospheric chemistry and physics, Environ Sci Technol, 39, 2668-2678, 10.1021/es0489137, 2005.
586 Rodigast, M., Mutzel, A., and Herrmann, H.: A quantification method for heat-decomposable methylglyoxal oligomers and its
587   application on 1,3,5-trimethylbenzene SOA, Atmos. Chem. Phys., 17, 3929-3943, 10.5194/acp-17-3929-2017, 2017.
588 Sato, K., Takami, A., Kato, Y., Seta, T., Fujitani, Y., Hikida, T., Shimono, A., and Imamura, T.: AMS and LC/MS analyses of
589   SOA from the photooxidation of benzene and 1,3,5-trimethylbenzene in the presence of NOx: effects of chemical
590   structure on SOA aging, Atmos. Chem. Phys., 12, 4667-4682, 10.5194/acp-12-4667-2012, 2012.
591 Shrivastava, M., Cappa, C. D., Fan, J. W., Goldstein, A. H., Guenther, A. B., Jimenez, J. L., Kuang, C., Laskin, A., Martin, S.
592   T., Ng, N. L., Petaja, T., Pierce, J. R., Rasch, P. J., Roldin, P., Seinfeld, J. H., Shilling, J., Smith, J. N., Thornton, J. A.,
593   Volkamer, R., Wang, J., Worsnop, D. R., Zaveri, R. A., Zelenyuk, A., and Zhang, Q.: Recent advances in understanding
594   secondary organic aerosol: Implications for global climate forcing, Rev. Geophys., 55, 509-559, 10.1002/2016rg000540,
595   2017.
596 Trostl, J., Chuang, W. K., Gordon, H., Heinritzi, M., Yan, C., Molteni, U., Ahlm, L., Frege, C., Bianchi, F., Wagner, R., Simon,
597   M., Lehtipalo, K., Williamson, C., Craven, J. S., Duplissy, J., Adamov, A., Almeida, J., Bernhammer, A. K.,
598   Breitenlechner, M., Brilke, S., Dias, A., Ehrhart, S., Flagan, R. C., Franchin, A., Fuchs, C., Guida, R., Gysel, M., Hansel,
599   A., Hoyle, C. R., Jokinen, T., Junninen, H., Kangasluoma, J., Keskinen, H., Kim, J., Krapf, M., Kurten, A., Laaksonen,
600   A., Lawler, M., Leiminger, M., Mathot, S., Mohler, O., Nieminen, T., Onnela, A., Petaja, T., Piel, F. M., Miettinen, P.,
601   Rissanen, M. P., Rondo, L., Sarnela, N., Schobesberger, S., Sengupta, K., Sipilaa, M., Smith, J. N., Steiner, G., Tome,
602   A., Virtanen, A., Wagner, A. C., Weingartner, E., Wimmer, D., Winkler, P. M., Ye, P. L., Carslaw, K. S., Curtius, J.,
603   Dommen, J., Kirkby, J., Kulmala, M., Riipinen, I., Worsnop, D. R., Donahue, N. M., and Baltensperger, U.: The role of
604   low-volatility organic compounds in initial particle growth in the atmosphere, Nature, 533, 527-+, 10.1038/nature18271,
605   2016.
606 Wang, S., Wu, R., Berndt, T., Ehn, M., and Wang, L.: Formation of Highly Oxidized Radicals and Multifunctional Products
607   from the Atmospheric Oxidation of Alkylbenzenes, Environ Sci Technol, 51, 8442-8449, 10.1021/acs.est.7b02374, 2017.
608 Watne, Å. K., Psichoudaki, M., Ljungström, E., Le Breton, M., Hallquist, M., Jerksjö, M., Fallgren, H., Jutterström, S., and
609   Hallquist, Å. M.: Fresh and Oxidized Emissions from In-Use Transit Buses Running on Diesel, Biodiesel, and CNG,
610   Environmental science & technology, 52, 7720-7728, 10.1021/acs.est.8b01394, 2018.
611 Vereecken, L., and Peeters, J.: A structure–activity relationship for the rate coefficient of H-migration in substituted alkoxy
612   radicals, 10.1039/C0CP00387E, 2010.
613 WHO: Ambient air pollution: A global assessment of exposure and burden of disease, 2016.
614 Wyche, K. P., Monks, P. S., Ellis, A. M., Cordell, R. L., Parker, A. E., Whyte, C., Metzger, A., Dommen, J., Duplissy, J.,
615   Prevot, A. S. H., Baltensperger, U., Rickard, A. R., and Wulfert, F.: Gas phase precursors to anthropogenic secondary
616   organic aerosol: detailed observations of 1,3,5-trimethylbenzene photooxidation, Atmos. Chem. Phys., 9, 635-665, DOI
617   10.5194/acp-9-635-2009, 2009.
618 Yan, C., Nie, W., Aijala, M., Rissanen, M. P., Canagaratna, M. R., Massoli, P., Junninen, H., Jokinen, T., Sarnela, N., Hame,
619   S. A. K., Schobesberger, S., Canonaco, F., Yao, L., Prevot, A. S. H., Petaja, T., Kulmala, M., Sipila, M., Worsnop, D.
620   R., and Ehn, M.: Source characterization of highly oxidized multifunctional compounds in a boreal forest environment
621   using positive matrix factorization, Atmos. Chem. Phys., 16, 12715-12731, 10.5194/acp-16-12715-2016, 2016.
622 Zhao, Y., Thornton, J. A., and Pye, H. O. T.: Quantitative constraints on autoxidation and dimer formation from direct probing
623   of monoterpene-derived peroxy radical chemistry, Proc. Natl. Acad. Sci. U. S. A., 115, 12142-12147,
624   10.1073/pnas.1812147115, 2018.
625